

## CHAPTER - III

Part A: A.C. Susceptibility Studies

Part B: Hysteresis

Part C: Initial Permeability

## Part A A.C. Susceptibility Studies

### 3.1 Introduction

A polycrystalline ferrite may contain multidomain (M.D.), single domain (S.D.) and super paramagnetic particles (S.P.) depending upon its thermal history. The studies on thermal variation of A.C. susceptibility explore the possibilities of existence of type of domains in the material. Using this technique many workers<sup>(1,2,3)</sup> have investigated the nature of magnetic domains in ferrites. In addition to the type of domain, the thermal variation of  $\chi_{a.c.}$  can also provide information about the type of anisotropy<sup>(4)</sup>. The influence of cation distribution on the magnetic properties of copper ferrites has been studied by Stierstadt et al<sup>(5)</sup>. They concluded that Curie temperature, the Hopkinson peak and tetragonal to cubic transition sensitivity depend upon the statistical distribution of the  $\text{Cu}^{2+}$  ions over the octahedral and tetrahedral sites. Recently Sawant et al<sup>(6)</sup> have reported bulk magnetic studies on Cu-Zn ferrites. They studied variation of  $\chi_{a.c.} - T$  variation and observed  $X/X_{RT}$  maximum for  $\text{CuFe}_2\text{O}_4$ . The maximum in  $\chi_{a.c.} - T$  variation is attributed to single (S.D.) to paramagnetic properties (S.P.) transition. Addition of  $\text{Zn}^{2+}$  leads to single domain (S.D.) + multidomain (M.D.) mixed state.

We have carried out studies on thermal variation of  $\chi_{a.c.}$  for the compositions  $Zn_{0.5}Cu_{0.5-t}Li_2Fe_2O_4$  where  $t = 0, 0.01, 0.02, 0.03, 0.04, 0.05, 0.06, 0.07,$  and  $0.08.$

### 3.2 Experimental

#### 3.2 a) Description of the Susceptibility apparatus

The schematic diagram of the apparatus is shown in figure (3.1). The set-up has the following parts.

- I) Helmholtz Coil (h, h) : Both the coils of 100 turns of 17 SWG super enamelled copper wire are wound on a wooden spool of mean diameter 74 cms. The two coils are firmly held on a wooden stand, such that they are separated by a distance equal to their radius.
- II) Pick-up Coil : This consists of two windings each having a large number of turns of 39 SWG super-enamelled copper wire wound in series position over a perspex spool and acts as the magnetic flux detector. The number of turns in them are so chosen that the emf generated in them in uniform time varying magnetic field annul each other. A third winding of about 500 turns is connected across a potentiometer of 10,000 Ohms, from which a variable voltage of either polarity can be obtained.

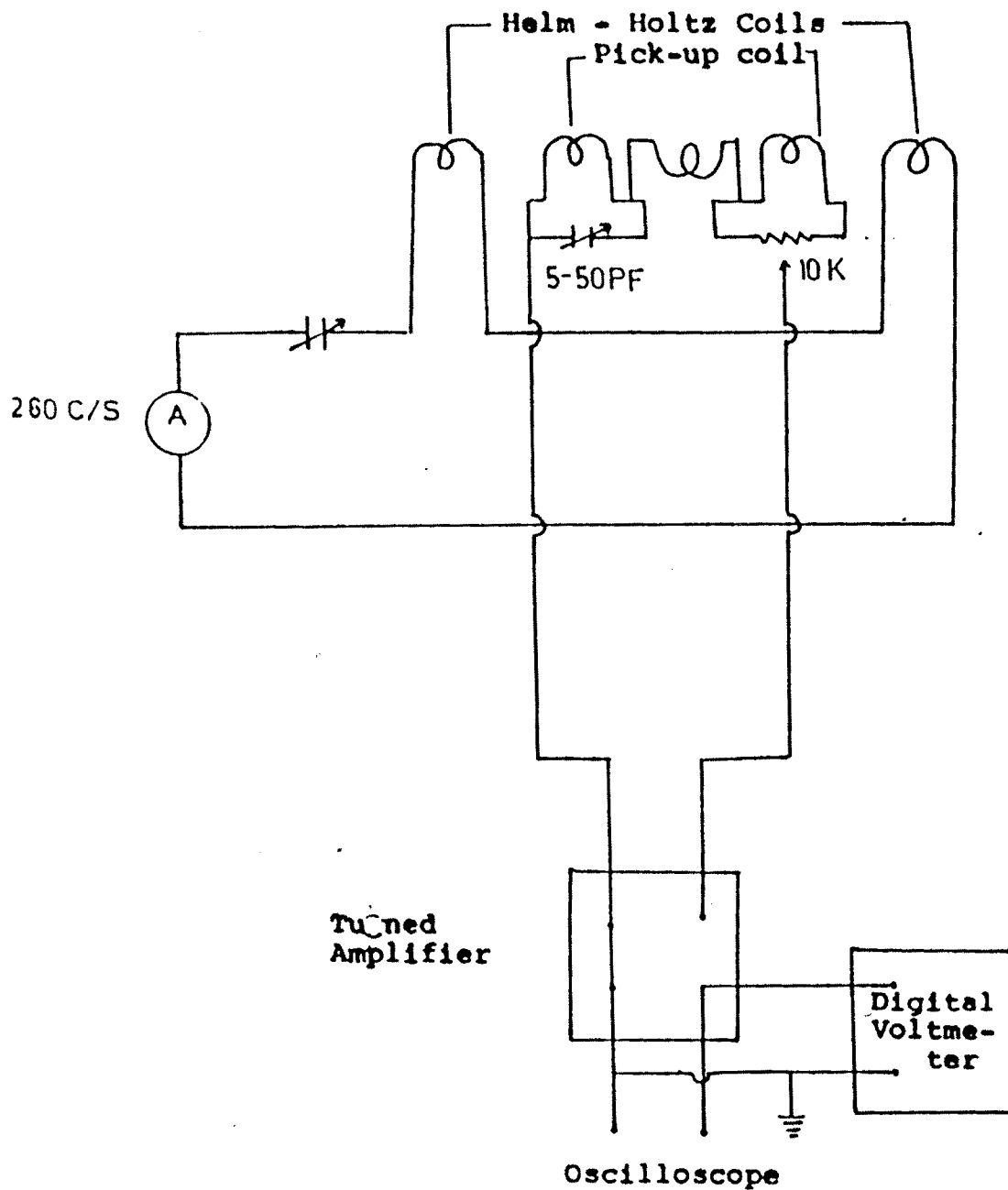


Fig. 3.1 : Schematic diagram of initial susceptibility apparatus.

This voltage of right polarity and magnitude is fed in series with the main windings. Since this cannot completely balance the emf due to a small phase difference arising out of the self capacities of the winding, a small trimmer capacitor of 5 to 50 P.F. is connected across the linear winding. When a nonuniform field due to an alternating dipole is produced near the coil system, a net emf in the coil proportional to the magnetic moment of the dipole is introduced. This principle is used for measuring the induced magnetic moment in magnetic materials. The emf induced in the pick-up coil for a magnetic moment depends upon two factors, namely, the dimensions of the double coil and the frequency of the alternating dipole and therefore, it is preferable to use a higher frequency of the applied magnetizing field for better sensitivity (however the use of high frequency is limited by the resonance effects in the double coil).

III) **Furnace** : This is made of platinum coil wound in a non-inductive way and supported inside a mullite tube of diameter 10 cm. Proper insulating is done from outside using asbestos sheets. The furnace is surrounded by a glass jacket through which cold water is circulated. This prevents the pickup coil from getting heated up when the furnace is switched on.

IV) **Sample holder** : It consists of a quartz tube of about 30 cm length and 2.5 cm diameter which can slide into the furnace. The quartz tube is almost closed by using plaster of paris after taking the thermocouple lead from inside the tube. A gap of about 2.3 cm from one end, where the thermocouple junction is fixed is left for positioning the sample close to the thermocouple. The quartz tube is supported on a wooden furnace and can be pushed in or pulled out of the furnace with ease.

V) **Temperature Measurements** : The thermocouple is of Pt/Pt - 10 % Rh. The emf is read on a digital multimeter.

### 3.2 b) Susceptibility Measurement

A specimen kept at the centre of a balanced double coil which itself is at the centre of a Helmholtz coil system producing an alternating magnetic field, behaves like an alternating dipole and induces a differential emf in the double coil. The current to the Helmholtz coil is supplied by an oscillator and a high quality power amplifier. The signal induced in the double coil which is proportional to the rate of change of magnetic moment of the specimen, is amplified, rectified and read out on a Digital Voltmeter (DVM). The sample was enclosed in a glass jacket containing the platinum-rhodium thermocouple to sense the temperature. The field was kept constant. The measurements were taken from room

temperature upto 400°C . The glass jacket containing the sample was removed slightly out of the heating arrangement intermittently to record the background effect. The magnetic moments were measured for different constant temperatures.

### 3.3 Results and Discussion

Bulk magnetic behaviour is generally comprehended in terms of domain structure. Temperature variation of A.C. magnetic susceptibility and hysteresis provide useful data on the domain structure. A crystalline ferrite material may contain

- i) Multi - domain (M.D.)
- ii) Single domain (S.D.) and
- iii) Super paramagnetic (S.P.),

particles depending upon the thermal treatment. When ferrites are prepared by ceramic method mixed domain states tend to be formed, resulting in the bulk magnetic properties appropriate to such mixtures. However in some ferrites M.D. or S.D. behaviour is determined primarily by composition and structure ( 4 ).

Grains containing domain walls within are termed multidomain (M.D.). These are large magnetic grains about tens of microns. Magnetic grains of size few hundred Å° or even large if the particles are circular cannot contain

domain walls. These are called single domain (S.D.). For these particles magnetization direction is fixed in space. Very small grains upto about hundred Angstroms ( $\text{\AA}$ ) are called super paramagnetic (S.P.). When thermal energy of S.D. particles becomes comparable to the effective magnetic anisotropy energy under the condition that magnetization direction fluctuates between the easy axes of the grains. The grains are then said to be exhibiting super paramagnetism. At this temperature  $T_b$  called blocking temperature the volume  $V$ , the saturation magnetisation  $J_s$  and coercive field  $H_c$  are related by Neel<sup>(7)</sup> as follows.

$$V J_s H_c = 2K T_b$$

where  $V$  is volume,  $J_s$  is saturation magnetization,  $H_c$  is coercive field and  $K$  is Boltzman constant.

Thus S.P. state can be changed to S.D. by cooling the ferrites below their  $T_b$ <sup>(8)</sup>.

#### Temperature Variation of Initial Susceptibility

For the samples in the form of pellets, lumps or micro powder, the apparent susceptibility  $X$  is related to the real susceptibility (Neel, 1995) as follows.

$$X = X^1 / (1 + NX^1)$$

where  $N$  is the demagnetizing factor.

Magnetisation measurements in low field typically less than 100 e and at high temperatures first carried out on iron by Hopkinson<sup>(9)</sup> revealed that it reaches a peak value just before  $T_c$  and becomes zero rapidly. Applying this technique C.R.K. Murthy et al<sup>(4)</sup> have explored complex magnetic behaviour of titanomagnetics R.S. Chaugule et al<sup>(10)</sup> have studied intermetallic compounds  $La_{1-x}Y_xMn_2Si_2$  by low field susceptibility method. Ferrites have been studied by this method by many workers<sup>(3)</sup>. Three types of peaks have been reported in  $\chi_{ac} - T$  curves as shown in figure ( 3.2 ).

#### 1) M.D. Particles

- i) Isotropic peak for the materials in the M.D. state provided the material has a temperature at which magnetocrystalline anisotropy is zero.
- ii) The  $\chi_{ac} - T$  does not show variation in the temperature region of investigation.

#### 2) S.D. Particles

S.D. peak occurs if the ferrite material has substantial proportion of S.D. particles in it and occurs at the  $T_b$  of the particles. If  $T_b$  is midway between  $T_R$  and  $T_C$  solid line curve results. Dashed curves are for the materials whose  $T_b$  is close to  $T_C$  as in figure ( 3.2 ). The Hopkinson peak has been explained by

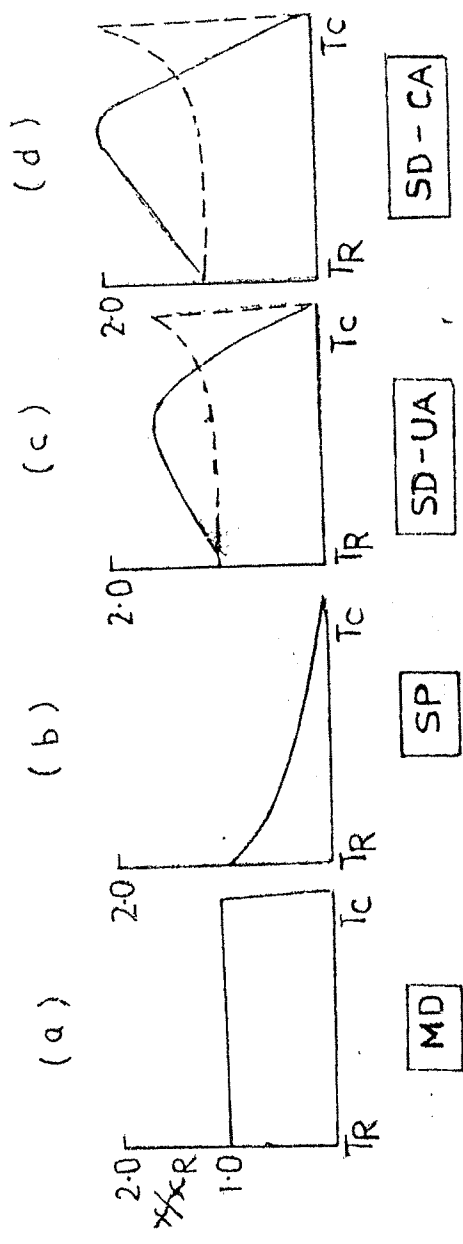


Fig. 3.2 : Normalised susceptibility versus temperature curves for series consisting of different domain stages.

C R.K. Murthy et al<sup>(7)</sup>. The rise in temperature diminishes the magnetic moment of the molecules gradually at first but more and more rapidly as the critical temperature at which magnetism disappearance is approached but the facility with which molecules have their axes directed increases with rise of temperature at first slowly but very rapidly indeed as the critical temperature is approached.

### 3) S.P. Particles

$\chi_{ac}$ , in case of S.P. particles, shows a continuous decrease with the increase of temperature and becomes zero at  $T_c$ .

Thus shapes of  $\chi_{ac} - T$  curve furnish information about the domain states of a particular sample as long as mixtures of several domain states are not involved.

In figures ( 3.3 ) and ( 3.4 ) thermal variations of normalized susceptibility for the compositions of  $Zn_{0.5}Cu_{0.5-t}Li_{2t}Fe_2O_4$  where  $t = 0, 0.01, 0.02, 0.03, 0.04, 0.05, 0.06, 0.07, 0.08$ , have been shown and the following observations are made.

- 1) All the compositions are temperature independent upto the Curie temperature. This is characteristic of M.D. type of grains.

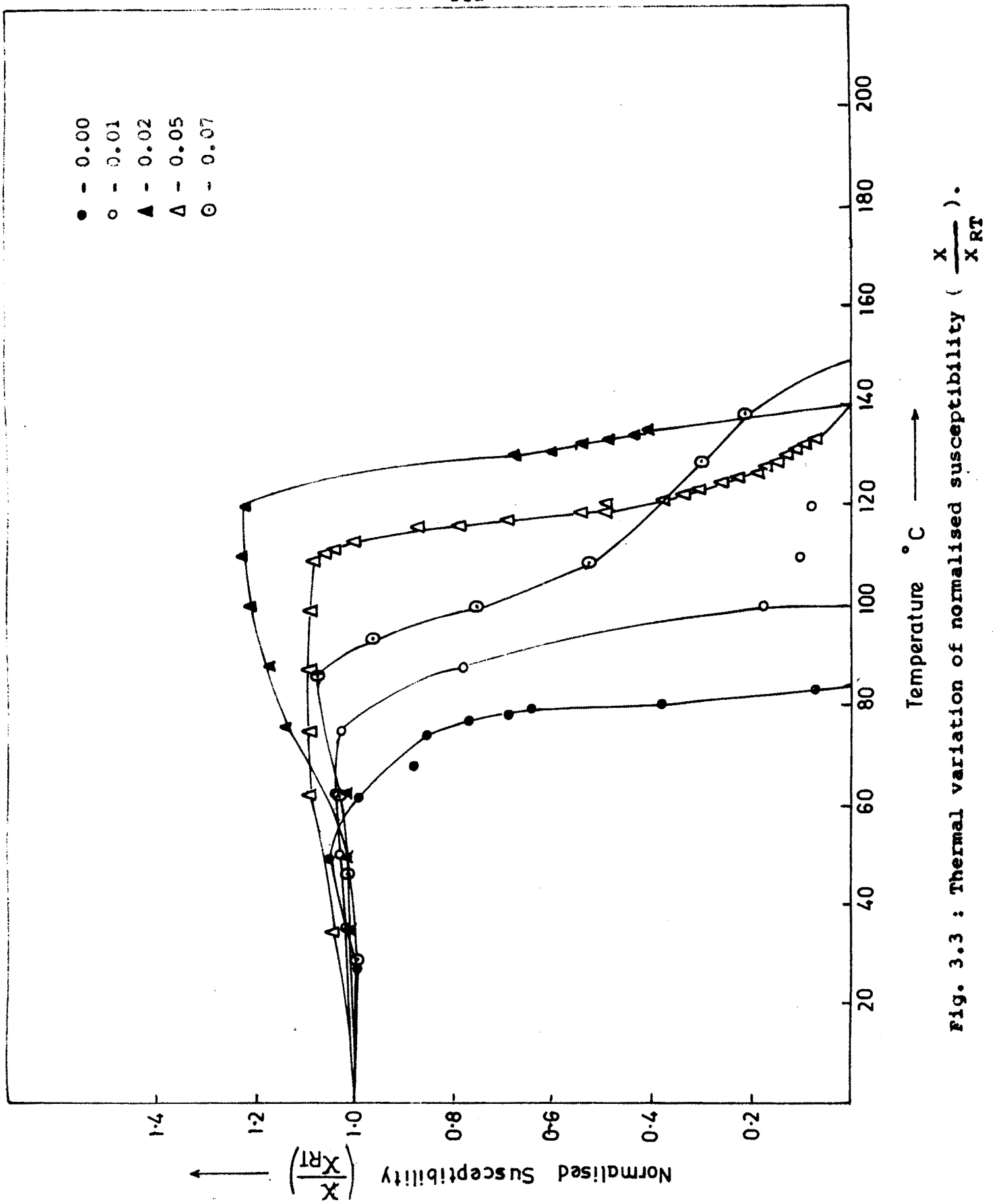


Fig. 3.3 : Thermal variation of normalised susceptibility  $\left(\frac{X}{RT}\right)$ .

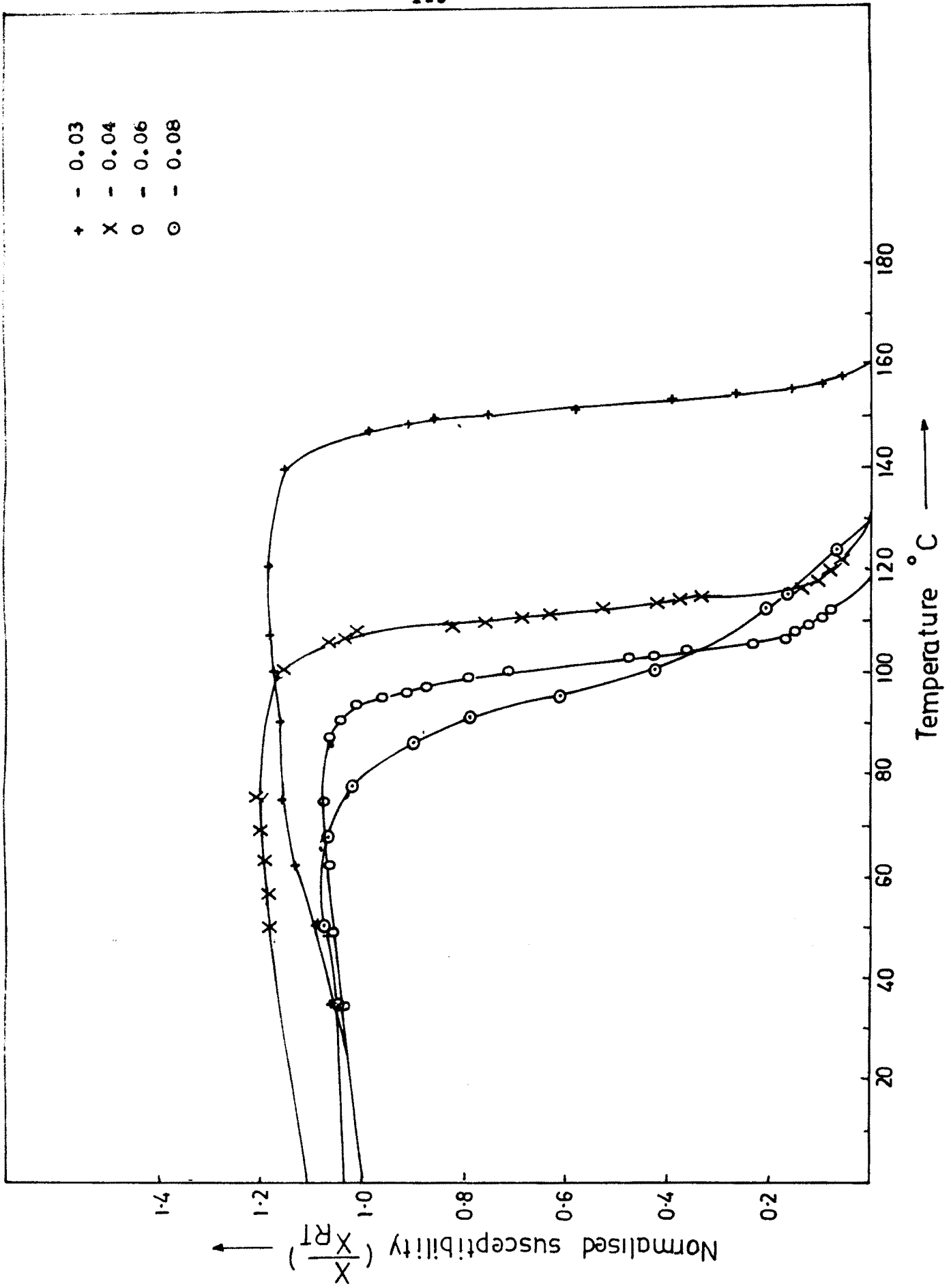


Fig. 3.4 : Thermal variation of normalised susceptibility ( $\frac{X}{RT}$ ).

- 2) Near the Curie temperature ( $T_c$ ),  $\chi_{ac}$  drops sharply and tends to zero.
- 3) Double  $T_c$  behaviour has not been observed in any of the compositions suggesting that all the compositions are single phase, as already confirmed from XRD analysis. For detail investigation the study of particle size distribution, would have thrown more light for clear analysis. However, looking at micrographs and average grain size data (Tab. 2.22) it can be concluded that there is dominance of M.D. type grains. But the peaking behaviour at high temperature indicates some S.D. grains.

The Curie temperature of the system increases on substitution of lithium. This can be explained on the basis of exchange interaction. It is seen that A - B exchange interactions become strong due to increased substitution of lithium ions by copper ions. The thermal energy required to offset the spin alignment increases which results in increase of Curie temperature with increase in lithium concentration.

## Part B Hysteresis

### 3B.1 Introduction

Magnetic hysteresis parameters like remanence ratio (R), coercive force ( $H_c$ ), saturation magnetisation ( $M_s$ ) are technologically important. The usefulness of a particular composition for particular application is decided by considering these parameters. For example, large squareness ratio is the requirement of the memory cores. The square loop ferrites are required for memory cores, phase shifters, shift registers, motors and generators. Soft ferrites are useful in electronic motors, loud-speakers, telephones and permanent magnets. In addition, the shapes of the hysteresis loop and thermal variation of retentivity and coercivity furnish information about the type of magnetic grains e.g. S.D., M.D. or S.P. is present in the material. This type of studies have been reported by some workers<sup>(4,10,11,12)</sup> Modulation of these parameters with various substituents in the mixed ferrites has also been studied and reported by some workers<sup>(13,14,15)</sup> We have carried out studies on magnetic hysteresis at 300°K using high field loop tracer.

### 3B.2 Experimental

3B.2 a) Alternating current electromagnet type hysteresis loop tracer.

The schematic diagram of the set up is shown in figure( 3.5 ). The essential parts of the instrument are,

- i) Electromagnet
- ii) Pick-up coil system
- iii) Balancing and integrating network and
- iv) Pre-amplifier

i) Electromagnet

The two C - cores of laminated grain - oriented silicon steel (English Electric Co. Type HWR/110/32 (13) of cross-section  $5 \times 2.5 \text{ cm}^2$  were used for this purpose. For one of the C - cores, a piece of 1.2 cm in thickness was cut out to get a pole gap of 1.2 cm. Then the two cores were joined together as shown in figure ( 3.5 ). The energising coil for the magnet consists of 2200 turns of 20 SWG super enamelled copper wire ( $R = 11.5 \text{ ohms}$ ) wound on a perspex former and firmly held together on a wooden base.

ii) Pick-up Coil System

A multicoil system which can be introduced in to the pole gap serves as a pick-up coil system. It consists of four different windings; one over the other wound with 39 SWG super - enamelled copper wire on a perspex former. The first winding ( $W_1$ ) has 2500 turns whereas the second ( $W_2$ ) has 1500 turns wound in opposite direction to that of  $W_1$ .  $W_1$  and  $W_2$  are connected in series and hence form the

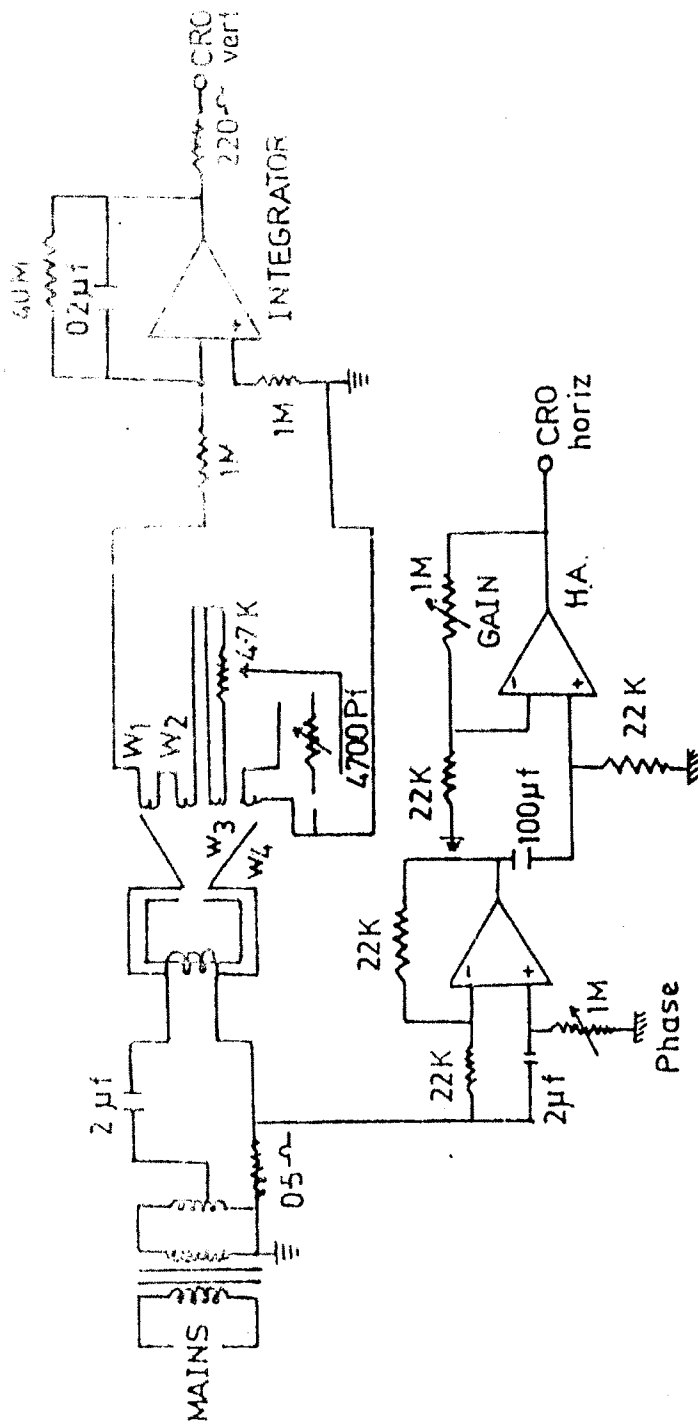


Fig.3.5 : Schematic diagram of hysteresis loop tracer

conventional double coil. The emf induced in  $W_1$  when placed in an alternating magnetic field can be brought very near to zero by adjusting the number of turns in  $W_2$ . Since this is difficult to achieve another winding  $W_3$  of 50 turns connected in series to  $W_2$  through a potentiometer is introduced. A fourth winding  $W_4$  of 5 turns has been included to avoid any ringing that could arise when a square loop magnetic sample is placed. The phase difference between the induced emf in  $W_1$  and  $W_2$  arising due to their self capacities has been corrected by connecting a suitable condenser across  $W_1$ .

The multicoin is connected through the balancing and integrating networks to an amplifier and then to the Y-plates of the oscilloscope. The input of the X-plates are taken from the emf developed across a resistance connected in series with the energising coil. A phase shifting network with proper inductance and variable resistance is also provided as shown in figure ( 3.5 ).

#### Sensitivity

When the pick field is 2400 Oe the peak to peak noise is of the order of 10 mV and a sample with magnetic moment of 1 emu would give sufficiently good hysteresis loops.

### 3B.2 b) Procedure of Measurement

The multicoil system was introduced into the pole gap. The coil wound on the C-core was energised by passing a suitable alternating current. This resulted in an alternating magnetic field in the pole gap and hence induction of emf in the multicoil, the potentiometer and the variable resistance in the balancing network were then adjusted to get a horizontal trace on the Oscilloscope. After reducing the current to zero, the multicoil was pulled out and the ferrite pellet kept at the central gap in the multicoil spool to be introduced into the pole gap. The current in the coil was increased to a value sufficient to saturate the sample photograph of the hysteresis loops on the oscilloscope screen were then taken.

Pure Nickel (99.9 %) in the form of a cylindrical pellet ( $\sigma_s = 54.30$  emu/gm) at 20°C was used for calibration of Y-axis. The horizontal scale was calibrated by measuring the field in the pole gap with a sensitive gauss meter while direct current were passed through the energising coil. For obtaining hysteresis loops, a.c. fields are used and hence the necessary corrections for d.c. field relation were incorporated.

### 3B.3 Results and Discussions

#### 3B.3.1) Compositional variation of magnetic moment $n_B$

The values of magnetic moment  $n_B$  have been calculated using the formula<sup>(8)</sup>.

$$n_B = \frac{\text{Molecular weight} \times M_s}{5585 \times d_s}$$

Where  $d_s$  is the density of the samples

$$M_s = (1 - P) \sigma_s d_s$$

$\sigma_s$  = Saturation magnetization in e.m.u./gm.

P = Porosity

In figure 3.6 variation of  $n_B$  as a function of lithium content is shown for  $Zn_{0.5}Cu_{0.5-t}Li_{2t}Fe_2O_4$ . It is seen that with the substitution of lithium there is gradual increase in  $n_B$ , it reaches maximum at ( $t = 0.05$ ) and for  $t > 0.05$  the  $n_B$  value decreases.

R.K. Puri et al<sup>(17)</sup> have reported magnetic studies of  $Ni_{0.4}Zn_{0.6-2x}Li_xFe_{2+x}O_4$ . They have observed substitution of  $Zn^{2+}$  ions by  $Li^{1+}$  ions resulting in increase of hyperfine field at octahedral as well as tetrahedral sites. Saturation magnetisation initially increases and then decreases with increased substitution of  $Zn^{2+}$  ions by  $Li^{1+}$  ions and  $Fe^{3+}$  ions. The result is explained on the basis of preferential site occupancy of different ions and their magnetic interactions.

Table 3.1 : Data on  $M_s$ ,  $n_B$ ,  $R$ ,  $D$ ,  $H_K^A$  and  $K_1$  for  
 $Zn_{0.5}Cu_{0.5-t}Li_{2t}Fe_2O_4$ .

t	$M_s$ emu/gm	$n_B$	$R = \frac{M_r}{M_s}$	D ( $\mu m$ )	$H_K^A$ Oe	$-K_1 \times 10^4$ ergs/cm <sup>3</sup>	$\alpha_{Y-K}$
0.00	189	1.53	0.75	2.64	310	3.00	60° 21' 53''
0.01	193	1.54	0.78	6.82	320	3.12	60° 39' 21''
0.02	208	1.65	0.77	4.32	310	3.24	59° 42' 36''
0.03	209	1.73	-	-	-	-	59° 13' 28''
0.05	231	1.85	0.79	8.67	430	3.72	58° 35' 57''
0.06	172	1.67	0.79	-	430	3.84	60° 10' 24''
0.07	192	1.54	0.83	11.00	440	3.96	61° 20' 17''
0.08	168	1.34	0.82	-	470	4.08	63° 1' 45''

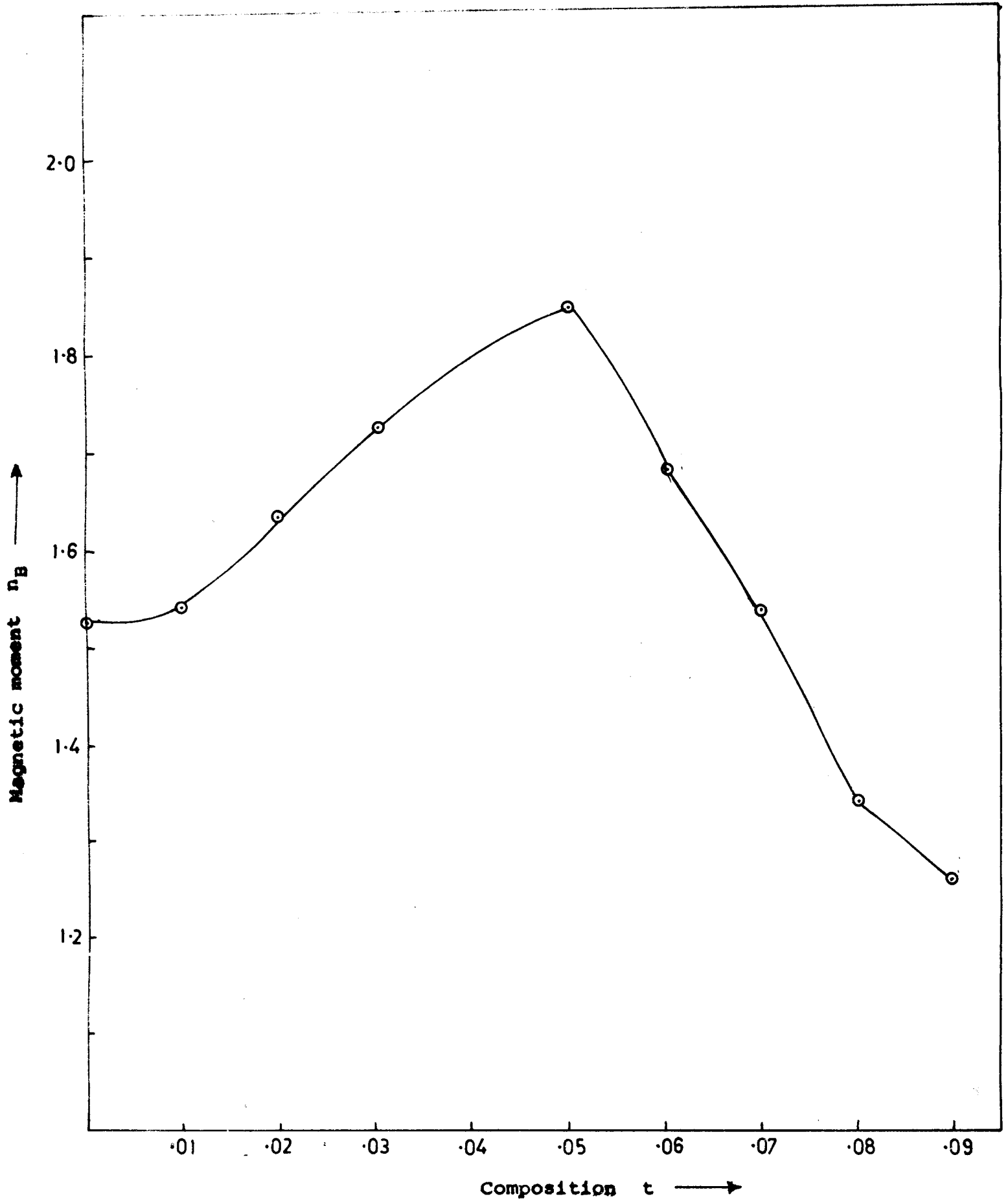


Fig. 3.6 : Compositional variation of magnetic moment ( $n_B$ )

The total magnetisation  $M$ , the Y-K angle  $\alpha_{YK}$ , the magnetic moment of A-sublattice  $M_A$  and the total magnetic moment of the B-sublattice  $M_B (=2M_{B1} = 2M_{B2})$  are related by the expression

$$M = M_B \cos \alpha_{YK} - M_A$$

According to site preference energies the copper ion always occupies B-site, while zinc ion occupies A-site in the spinel. Argentina and Baba<sup>(18)</sup> have shown that in lithium ferrite the octahedral site is dominant for the reduction or elevation of saturation magnetization.

From table 3.1 it is clear that as the content of lithium is increased, canting angle decreases and then increases up to a certain concentration. Srivastava et al<sup>(19)</sup> have found existence of Yafet-kittel angles in Cu-Zn and Fe-Zn ferrite system. It is believed that the change in magnetization on lithium substitution occurs due to the presence of Yafet-kittel angle in the spin system on B-sites. The variation of  $n_B$  with lithium concentration is according to Yafet-kittel theory.

### 3B.3 ii) Magnetocrystalline anisotropy field ( $H_K^A$ )

The energy necessary to turn the magnetization out of preferred direction to the hard direction is called magneto-crystalline energy. Magneto-crystalline energy will depend upon the angles between the magnetization vectors and crystal axes, as well as strength with which the magnetization is bound to the easy axis.

A cubic crystal possesses crystal anisotropy energy  $E_A$ .

$$E_A = K_0 + K_1 (l^2 m^2 + m^2 n^2 + n^2 l^2) + K_2 (lmn)^2$$

$K_0$  - Value of minimum energy position

$K_1$  - Anisotropy constant of (110) direction

$K_2$  - Anisotropy constant of (111) direction

$l$  - Projection of unit magnetization vector on X-axis

$m$  - Projection of unit magnetization vector on Y-axis

$n$  - Projection of unit magnetization vector on Z-axis

When the easy direction of magnetization is parallel to a cubic edge (100), then  $E_A = K_0 = 0$

The anisotropy field is given by

$$H_K^A = \frac{2K_1}{M_S}$$

Magneto-crystalline energy is solely a function of crystal structure and chemical composition and is independent of microstructure. Table 3.1 summarises data on  $H_K^A$  for the

various composition of  $Zn_{0.5}Cu_{0.5-t}Li_{2t}Fe_2O_4$ . It is seen that with the substitution of lithium the anisotropy field goes on increasing. The anisotropy field is given by above equation.

To understand the variation of  $H_K^A$ , behaviour of  $K_1$  must be understood.

### 3B.3 iii) Magnetocrystalline Anisotropy Constant ( $K_1$ )

The magnitude of the magnetocrystalline anisotropy constant  $K_1$  represents the extent to which the magnetization of an individual grain favours particular crystallographic directions (easy axes). In other words it is a measure of the energy required to rotate the magnetization from an easy to a hard direction. The constant  $K_1$  is related to coercive force, saturation magnetization, remanence ratio, domain wall energies etc., therefore it is an important parameter. In terms of domain walls, the effect of an increasing  $K_1$  means to raise the domain wall energies. It is known that influence of temperature on  $K_1$  is felt in two ways.

- i) temperature dependence of basic mechanism of  $K_1$  and
- ii) the change in anisotropy due to temperature variation of the saturation magnetization.

The influence of temperature variation of  $M_s$  on that of  $K_1$  was predicted by Zener<sup>(20)</sup> as,

$$K_1(T) = K_1(0) \left( \frac{M_s}{M_0} \right)^{10}$$

A similar third power law holds for uniaxial anisotropy. Thus effective decrease in  $K_1$  with temperature is much faster than that in  $M_s$  with temperature.

Table 3.1 summarises data on anisotropy constant  $K_1 \times 10^4$  ergs/cm<sup>3</sup>. The values of  $K_1$  are calculated by taking the end values of the corresponding ferrites and taking into consideration the stoichiometry of the composition. It is seen that  $K_1$  increases with the addition of  $Li^{1+}$ , which suggests that more energy is required to turn the magnetization vector from easy to hard direction.

### 3B.3 iv) Remanence Ratio (R)

The remanence ratio and coercive force depend on microstructure, temperature, magnetocrystalline anisotropy and stress sensitivity. Each of these can have a profound effect on the loop shape either independently or combined. In addition, the anisotropy and stress effects are temperature dependent. The remanent magnetization is determined to a large extent by the nucleation of reverse or 90° spike domains about a pore or grain boundary. As a consequence the size of any spike domains will directly contribute to a reduction in  $R^{(21)}$  Coercive force and Remanence ratio

depend on the size and growth of magnetic domains. The effect of magnetic anisotropy and stress on domain wall energy must be considered. The magnitude of anisotropy constant is the measure of energy required to rotate the magnetization from easy direction to a hard direction. The relation between  $R$  and  $K_1$  is not very clear. An analysis of the effect of anisotropy on spike domain size has revealed that the reduction in  $R$  from spike domains should increase with  $K_1/A$ . However, nucleation field for reverse domain is expected to create a favourable remanence when the magnitude of  $K_1$  is increased, as predicted by Goodenough<sup>(22)</sup>.

Table 3.1 summarises data on remanence ratio of  $Zn_{0.5}Cu_{0.5-t}Li_{2t}Fe_2O_4$ . It is observed that  $R$  increases with the addition of lithium ion concentration. Increase of  $R$  appears to be due to increase in  $K_1$ .

### Part C Initial Permeability

#### 3C.1 Introduction

The magnetic permeability may be considered to be a measure of efficiency of a magnetic material<sup>(23)</sup>. In metallic magnetic materials that have higher saturation magnetization than ferrites, the highest permeabilities are not usually present in material with highest saturations. Studies on thermal and frequency variations of initial permeability of ferrite furnish valuable information about domain nature<sup>(4)</sup>, Curie temperature<sup>(24)</sup>, and the factors contributing to the permeability changes<sup>(25)</sup>. Therefore, these studies are important. Besides the theoretical importance, knowledge of initial permeability is also essential from the application point of view of the ferrite material e.g. for the antenna rods of A.M. broadcast receiver, the permeability value must be moderate (150 - 500)<sup>(26)</sup>. High permeabilities can provide high energy, storage at lower current and reduced component volume, a characteristic necessary for inductor chokes, coils, filters and resonant circuits<sup>(27)</sup>.

The initial permeability is defined as,

$$\mu_1 = \left( \frac{1}{\mu_0} \right) \lim_{H \rightarrow 0} \frac{B}{H}$$

where  $\mu_0$  - Permeability in vacuum

$\mu_1$  - Dimensionless quantity

$\mu_1$  is a complex quantity denoted as,

$$\mu_1 = \mu' - j\mu''$$

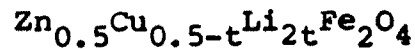
The real part  $\mu'$  describes stored energy and imaginary part  $\mu''$  describes dissipation. The loss factor is given by,

$$\tan \delta = \mu'' / \mu'$$

Initial permeability increases with increase in temperature falling abruptly close to Curie point<sup>(28)</sup>. The use of very pure materials and composition within a narrow region of zero crystalline anisotropy and zero magnetostriction, when processed under carefully controlled condition results in a very sharp peak in  $\mu_1 - T$  curve<sup>(27)</sup>. From practical point of view, steep rise and steep drop in permeability within a narrow temperature range are not desirable, instead one needs a reasonably high and uniform permeability over a broad temperature range of 20°C to 60°C<sup>(29)</sup>.

Few workers<sup>(30-33)</sup> have shown that in ferrites  $\mu_1$  increases with temperature up to Curie point or reaches a maximum value at the temperature where the anisotropy constant changes sign.

We have carried out work on thermal and frequency variation of initial permeability of the system



$t = 0, 0.01, 0.02, \dots, 0.3$

The results are discussed with the help of theory.

### 3C.2 Experimental

We have measured the initial permeability as a function of temperature at 10 KHz over the temperature range from room temperature to 400°C using an HP-4275 A LCRQ meter (20 Hz to 1 MHz). The furnace was temperature regulated with  $\pm 2^\circ\text{C}$  error in the temperature range.

The permeability as a function of frequency at room temperature was measured over the frequency range from 20 Hz to 1 MHz.

The initial permeability was calculated from the low field inductance measurements with torroidal core of 100 turns using the formula.

$$L = 0.0046 \mu_1 N^2 h \log d_2/d_1$$

where  $L$  is the inductance in  $\mu\text{H}$

$d_2$  is the outer diameter

$d_1$  is the inner diameter

$\mu_1$  is the initial permeability of the core

$h$  is the height of the core in inches

### 3C.3 Results and Discussion

#### 1) Compositional Variation of Initial Permeability :

In figure(3.7) variation of initial permeability with the content of  $\text{Li}^{1+}$  in  $\text{Zn}_{0.5}\text{Cu}_{0.5-t}\text{Li}_{2t}\text{Fe}_2\text{O}_4$  are shown. It is clearly seen that there is a decrease in  $\mu_i$  with the substitution of  $\text{Li}^{1+}$ . According to Globus model<sup>(34)</sup>,

$$\mu_i \approx \frac{M_s^2 D}{K_1}$$

where  $\mu_i$  is the initial permeability

$M_s$  is the saturation magnetization

$D$  is the average grain size

and  $K_1$  is the magnetocrystalline anisotropy

As it has been observed from hysteresis studies, that  $M_s$  increases initially and then decreases, and the grain size has been found to increase with increase of concentration of  $\text{Li}^{1+}$  ions, also the magnetocrystalline anisotropy increases. The decrease of  $\mu_i$  with incorporation of  $\text{Li}^{1+}$  ions can be attributed to increase in  $K_1$  magnetocrystalline anisotropy which seems to be more dominant in the equation. Similar observations have been made by Puri et al<sup>(17)</sup>.

In table 3.3 data on initial permeability ( $\mu_i$ ), wall permeability ( $\mu_w$ ), rotational permeability ( $\mu_{RK}$ ), average grain size ( $D$ ), initial susceptibility ( $\chi_{int}$ ), are given.

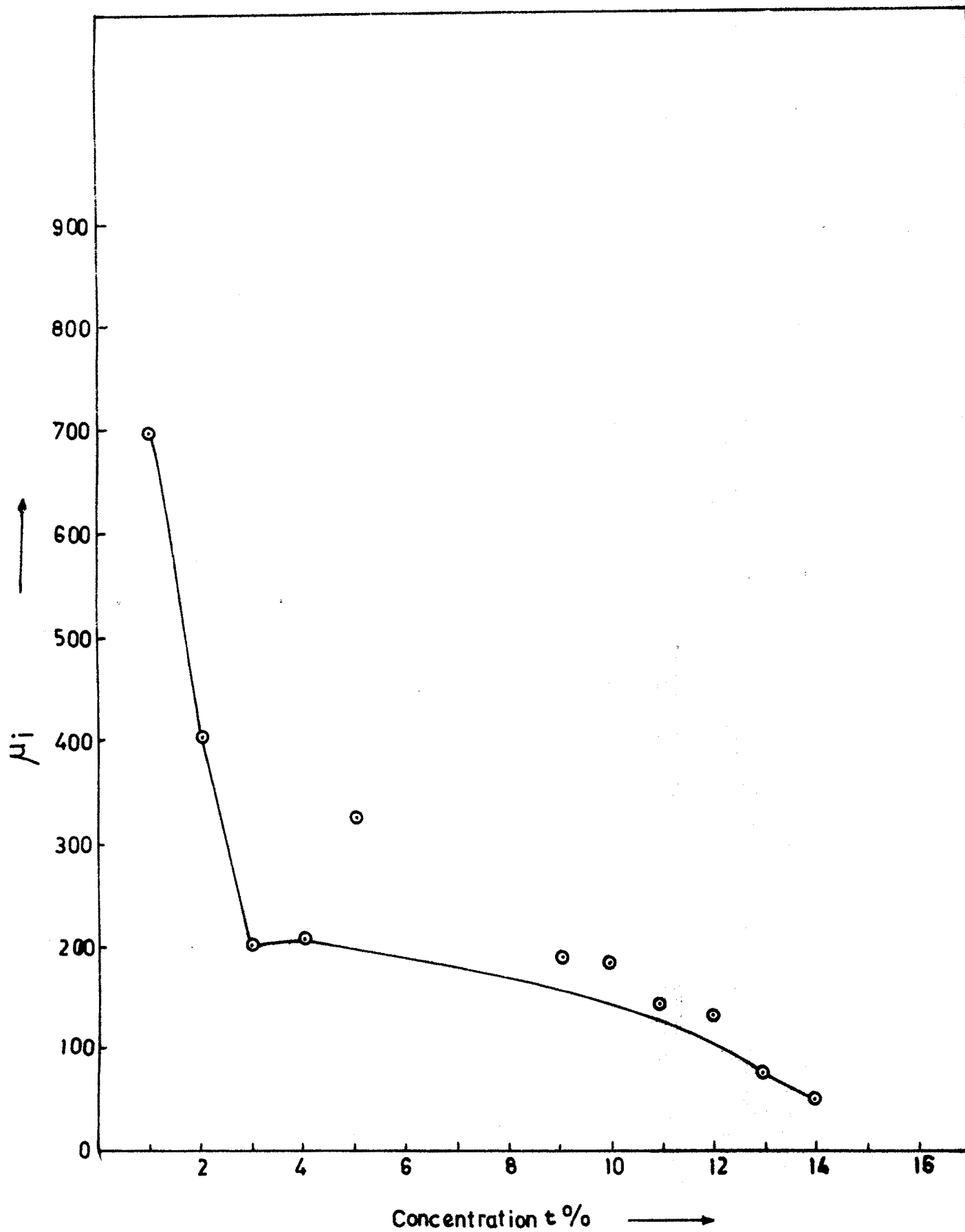


Fig. 3.7 : Compositional variation of initial permeability ( $\mu_1$ ).

Table 3.3 : Data on initial permeability ( $\mu_i$ ), wall permeability ( $\mu_w$ ), rotational permeability ( $\mu_{rK}$ ), average grain size (D), initial susceptibility ( $X_{int}$ ) for the  $Zn_{0.5}Cu_{0.5-t}Li_{2t}Fe_2O_4$

t	$\mu_i$	$\mu_w$	$\mu_{rK}$	$X_{int} = \frac{\mu_i - 1}{4\pi}$	$-K_1 \times 10^4$ ergs/cm <sup>3</sup>
0.00	699	268	8	56	3.00
0.01	401	150	8	32	3.12
0.02	202	71	9	16	3.24
0.03	210	74	9	17	3.36
0.04	324	122	7	26	3.48
0.05	414	118	10	33	3.60
0.06	380	158	6	30	3.72
0.07	283	143	7	22	3.84
0.08	179	107	5	14	3.96
0.09	189	50	6	15	4.08
0.10	142	51	4	12	4.20

The values of rotational permeability  $\mu_{rk}$  have been calculated using the formula given<sup>(15)</sup>

$$\mu_{rk} - 1 = \frac{2}{3} (1 - p) \frac{4 \pi M_s}{H_K^A}$$

The wall permeability  $\mu_w$  is given by the relation

$$\mu_w = \mu_i - (\mu_{rk} - 1)$$

There is a relationship between  $\mu_w$  and  $\mu_{rk}$  which is

$$\mu_w = \mu_{rk}^{\alpha}$$

From table 3.3 it is seen that the magnitude of wall permeability  $\mu_w$  is greater than the magnitude of rotational permeability. Thus in all the compositions, the main contribution to the initial permeability is due to domain wall motion. It is also seen that with addition of lithium ion the wall permeability  $\mu_w$  decreases. This suggests that these ions cause impedance to the domain wall motion and that more the concentration of these ions more is the obstruction to the wall motion.

Table 3.4 : Curie temperature values determined from A.C. Susceptibility and initial permeability study.

Composition t	From A.C. Susceptibility $T_C$ ( $^{\circ}\text{C}$ )	From Initial permeability $T_C$ ( $^{\circ}\text{C}$ )
0.00	85	90
0.01	100	100
0.02	140	140
0.05	130	140
0.07	150	150

### ii) Thermal Variation of Initial Permeability :

In figures 3.8 to 3.10 thermal variation of initial permeability  $\mu_i$ , its real part  $\mu'$ , and imaginary part  $\mu''$  for the compositions  $\text{Zn}_{0.5}\text{Cu}_{0.5-t}\text{Li}_{2t}\text{Fe}_2\text{O}_4$  are shown in the temperature range from room temperature up to Curie temperature  $T_c$  for the few compositions. It is observed that  $\mu_i$  and  $\mu'$  increase (slightly) with temperature up to Curie temperature ( $T_c$ ). Near  $T_c$ , there is a sharp drop of  $\mu_i$  and  $\mu'$  to zero. Sharp decrease in  $\mu_i$  and  $\mu'$  suggests single phase formation of the ferrite material. This observation supports the conclusions drawn from the XRD analysis that all the compositions are single phase.

In most of the magnetic materials  $\mu_i$  increases with temperature up to Curie temperature. This is because the anisotropy field usually decreases faster with temperature than  $M_s$  (16). When the magnetocrystalline anisotropy constant ( $K_1$ ) passes through zero the permeability rises to a peak value. Enz (35) and Ohta (36) both have shown that the initial permeability  $\mu_i$  shows a maximum value at the temperature where the anisotropy constant  $K_1$  changes the sign.

We have concluded from the  $X_{a.c.} - T$  curves that all the compositions investigated contain predominantly

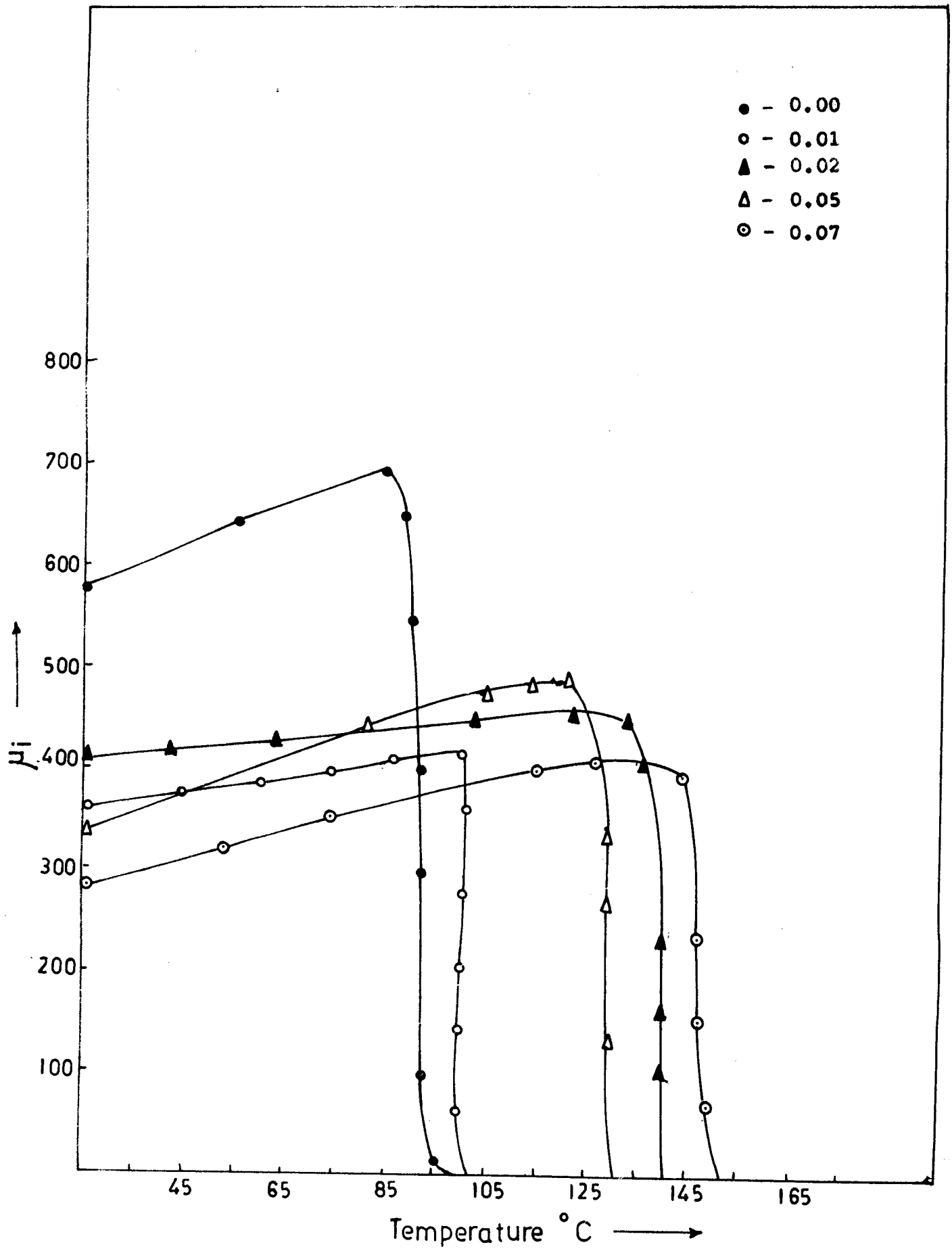


Fig. 3.8 : Variation of initial permeability with temperature

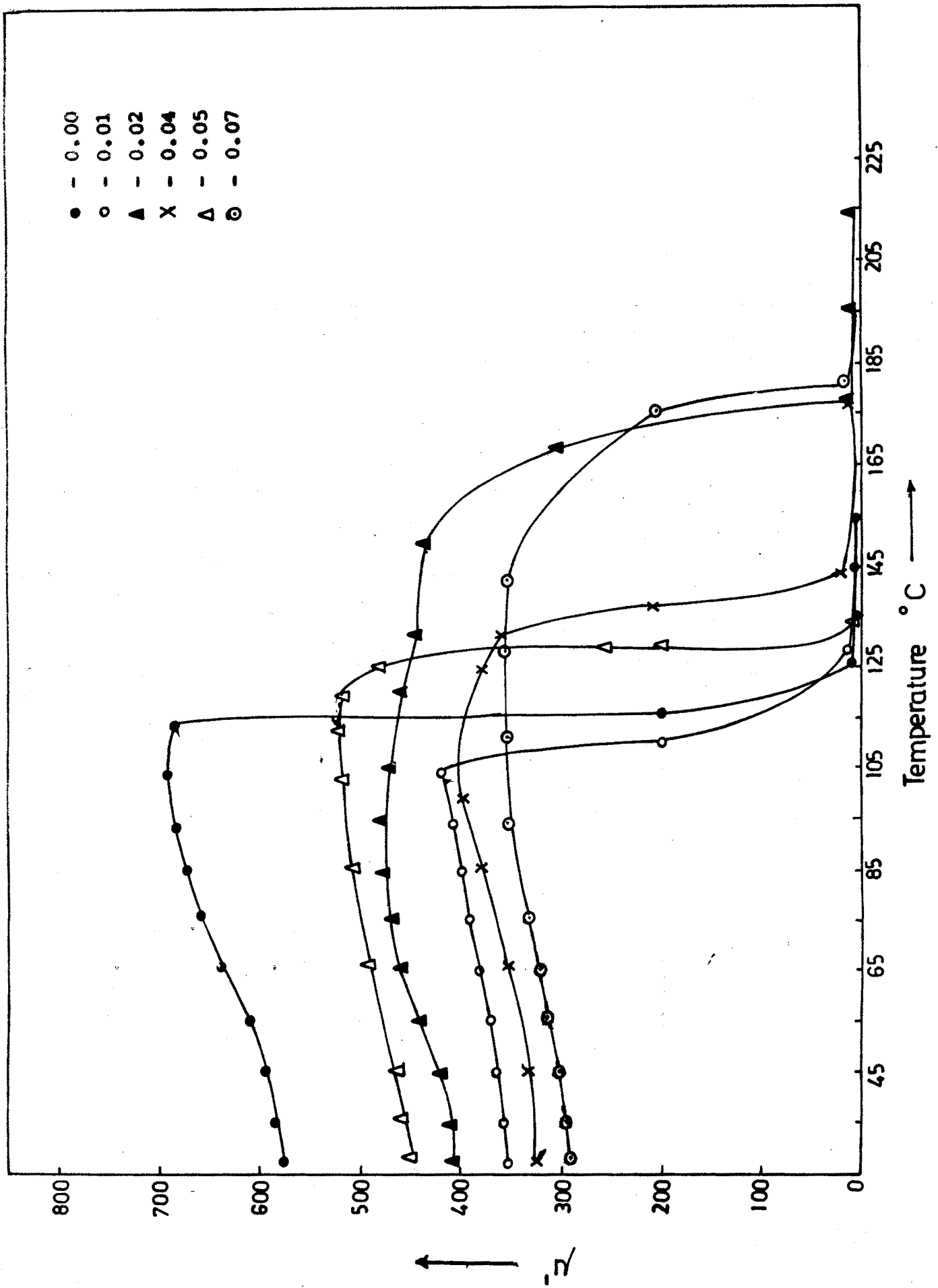


Fig. 3.9 : Thermal variation of ( $\chi$ ) for  $Zn_{0.5}Cu_{0.5-t}Li_2tFe_2O_4$ .

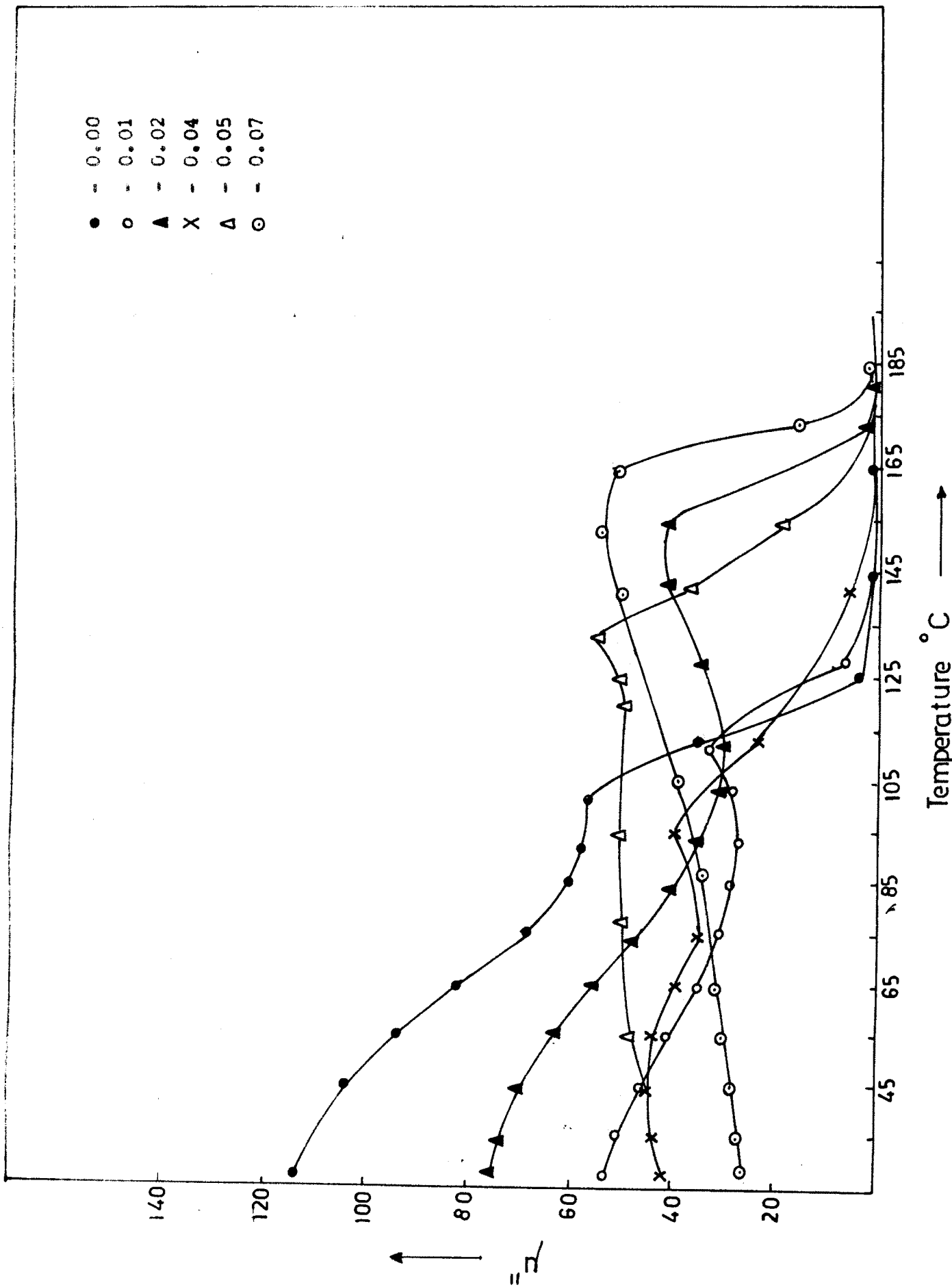


Fig. 3.10 : Thermal variation of ( $\chi''$ ) for  $Zn_{0.5}Cu_{0.5-t}Li_2tFe_2O_4$ .

M.D. grains. However, small peaks have been explained on the basis of average, grain size distribution. The indication of peak suggests the presence of some S.D. grains.

Thus  $\mu_1 - T$  curves resemble with  $X_{a.c.} - T$  curves. The Curie temperature values determined from  $X_{a.c.} - T$  and  $\mu_1 - T$  studies are given in table ( 3.4 ).

As already evidenced from SEM studies that average grain size distribution favours M.D. grains. However, there is presence of some S.D. grains which tend to exhibit their behaviour at elevated temperatures giving rise to small peaks. This behaviour is exhibited in most of the compositions of  $\mu_1$  and  $\mu''$  thermal variation. Thus in general the materials exhibit M.D. type of behaviour but the role of S.D. grains become significant at high temperature as seen from  $\mu_1, \mu'' - T$  curves.

From thermal variation of  $\mu''$ , it is seen that with increase of temperature,  $\mu''$  increases, reaches maximum near  $T_c$  and then falls sharply near  $T_c$ , for  $t = 0.06, 0.07$  indicating increase loss in these compositions. Where as for  $t = 0, 0.01, 0.02$ ,  $\mu''$  decreases with temperature indicating decrease of loss for these compositions. The increase in loss is due to thermal randomisation.

### 3C.3 iii) Frequency Dependence of Initial Permeability :

In figure 3.11 and 3.12 variation of  $\mu'$  and  $\mu''$  with frequency in the range 20 Hz to 1 MHz for the compositions of  $\text{Zn}_{0.5}\text{Cu}_{0.5-t}\text{Li}_{2t}\text{Fe}_2\text{O}_4$  are shown.

In ferrimagnetic materials, the initial permeability is believed to arise from the reversible domain wall motion and rotation of spin within domains. Contribution to  $\mu_i$  from spin rotation is small on account of high magneto-crystalline anisotropy. The value of  $\mu_i$  is greatly influenced by the method of preparation, firing temperature and porosity. The pores present hinder domain wall motion, leading to the decrease in  $\mu_i$ . In addition, the pores give rise to local demagnetizing fields which are expected to modify the domain pattern near to the boundary.

Rado<sup>(37)</sup> and others<sup>(38-40)</sup> observed high frequency dispersion and absorption in  $\mu_i$  and attributed it to rotational resonance in the combined anisotropy and demagnetizing fields while the low frequency dispersion was attributed to domain wall displacements. Single domain particles did not exhibit low frequency dispersion confirming the hypothesis of low frequency dispersion in  $\mu_i$  to be due to domain wall movement.

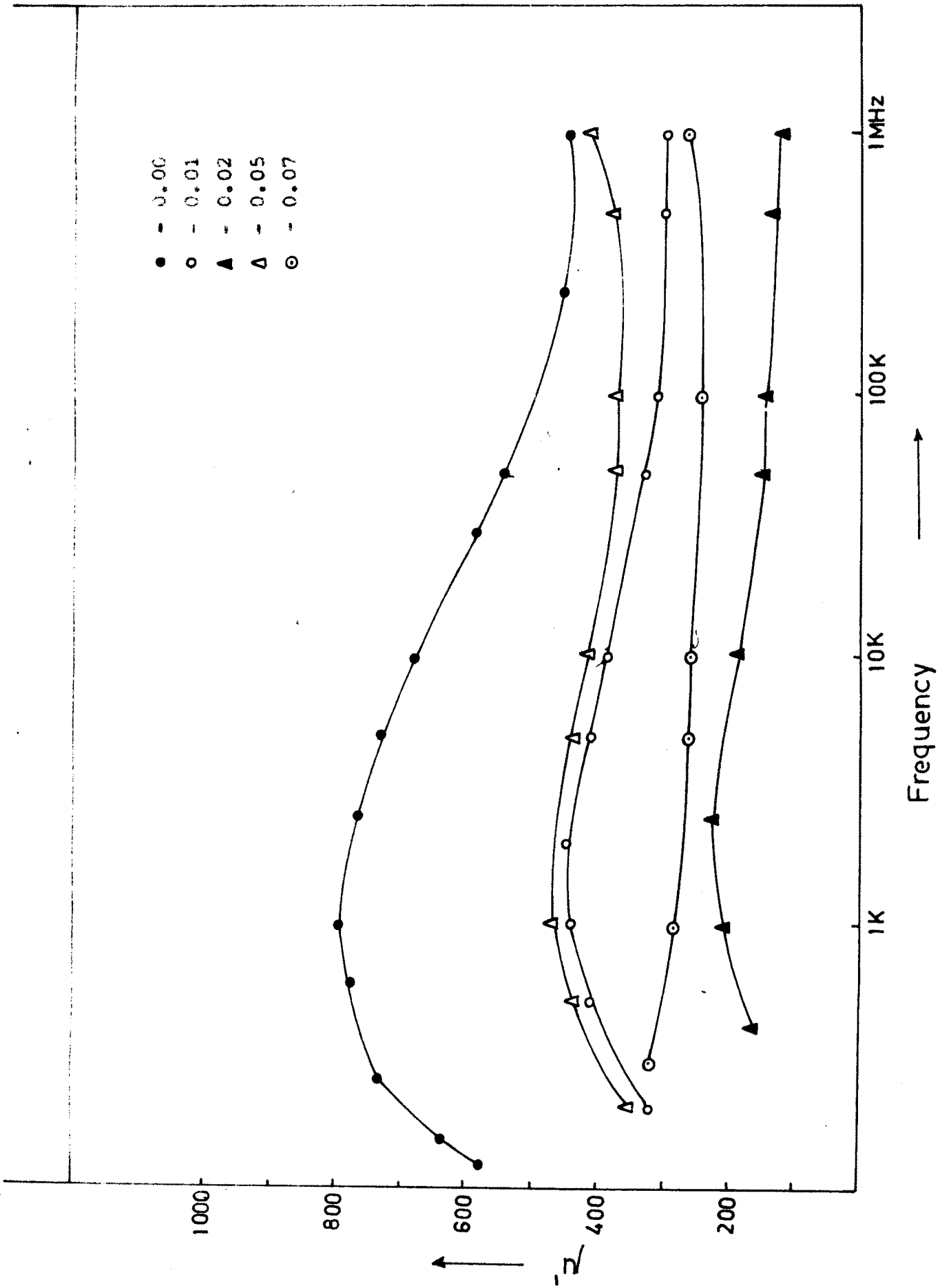


Fig. 3.11 : Frequency variation of ( $\mu'$ ) for  $Zn_{0.5}Cu_{0.5-t}Li_{2t}Fe_2O_4$

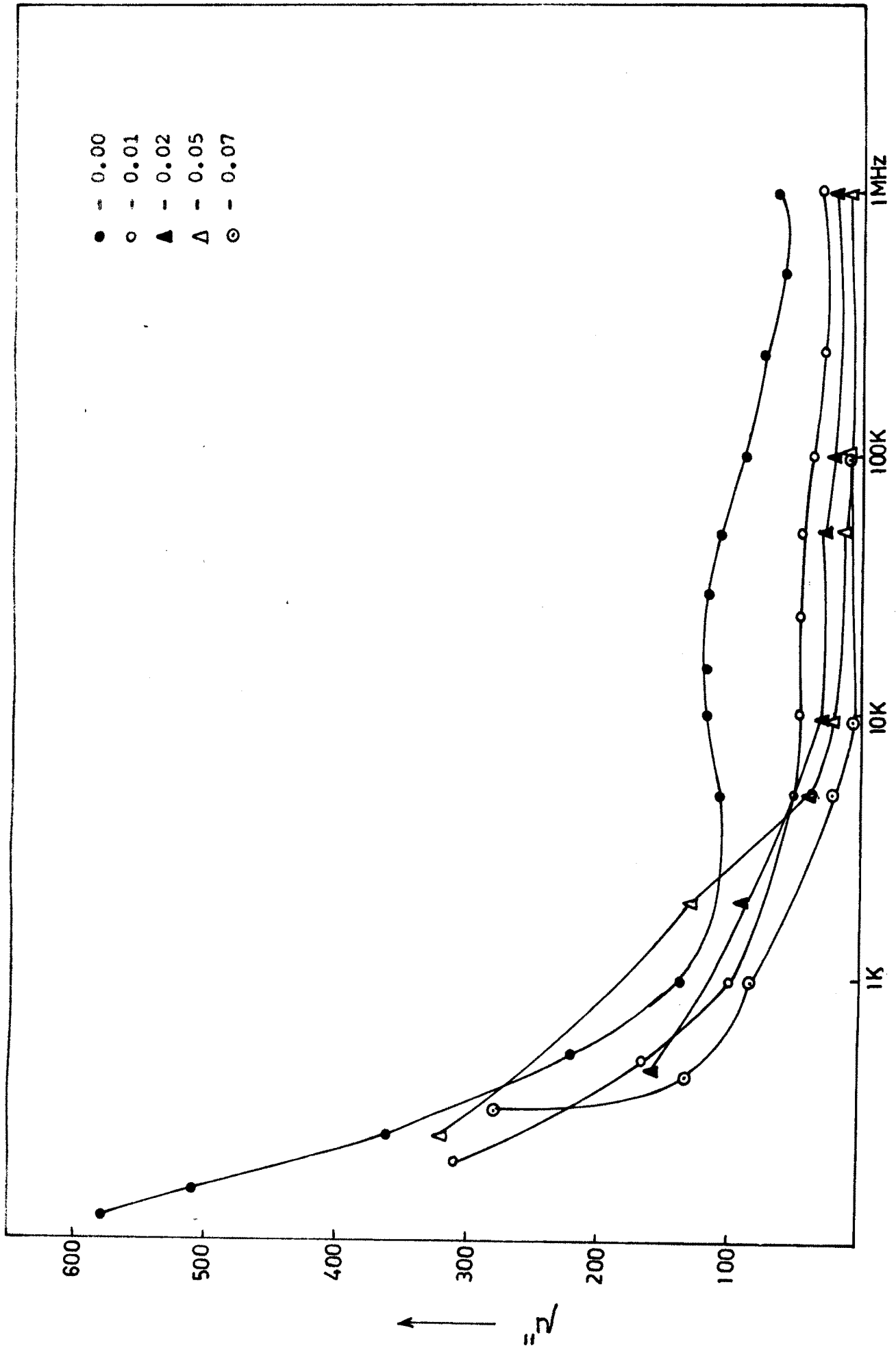


Fig. 3.12 : Frequency variation of ( $\mu''$ ) for  $Zn_{0.5}Cu_{0.5-t}Li_2tFe_2O_4$ .

In figures 3.11 and 3.12 frequency variation of  $\mu'$  and  $\mu''$  clearly indicate the low frequency dispersion which may be attributed to the domain wall movements. We have already shown that the contribution to  $\mu_1$  arises mainly from  $\mu_{\omega}$ , which supports these observations.

### 3C.3 iv) Loss Factor (L.F.) :

The ratio of the imaginary part of the permeability representing the losses in the material to the real part of the permeability is a measure of the inefficiency of the magnetic system. It is called the loss tangent.

$$\text{Loss tangent} = \tan \delta = \frac{\mu''}{\mu'}$$

The loss tangent per unit of permeability is called the loss factor (L.F.)

$$\text{L.F.} = \frac{\tan \delta}{\mu_1}$$

This factor parameter should be as low as possible.

In figure 3.13 dispersions of L.F. for the compositions  $\text{Zn}_{0.5}\text{Cu}_{0.5-t}\text{Li}_{2t}\text{Fe}_2\text{O}_4$  are shown. With the increase of frequency from 50 Hz to 10 KHz, the L.F. decreases. In most of the compositions, the L.F. value is invariant to frequency variation above 10 KHz. The

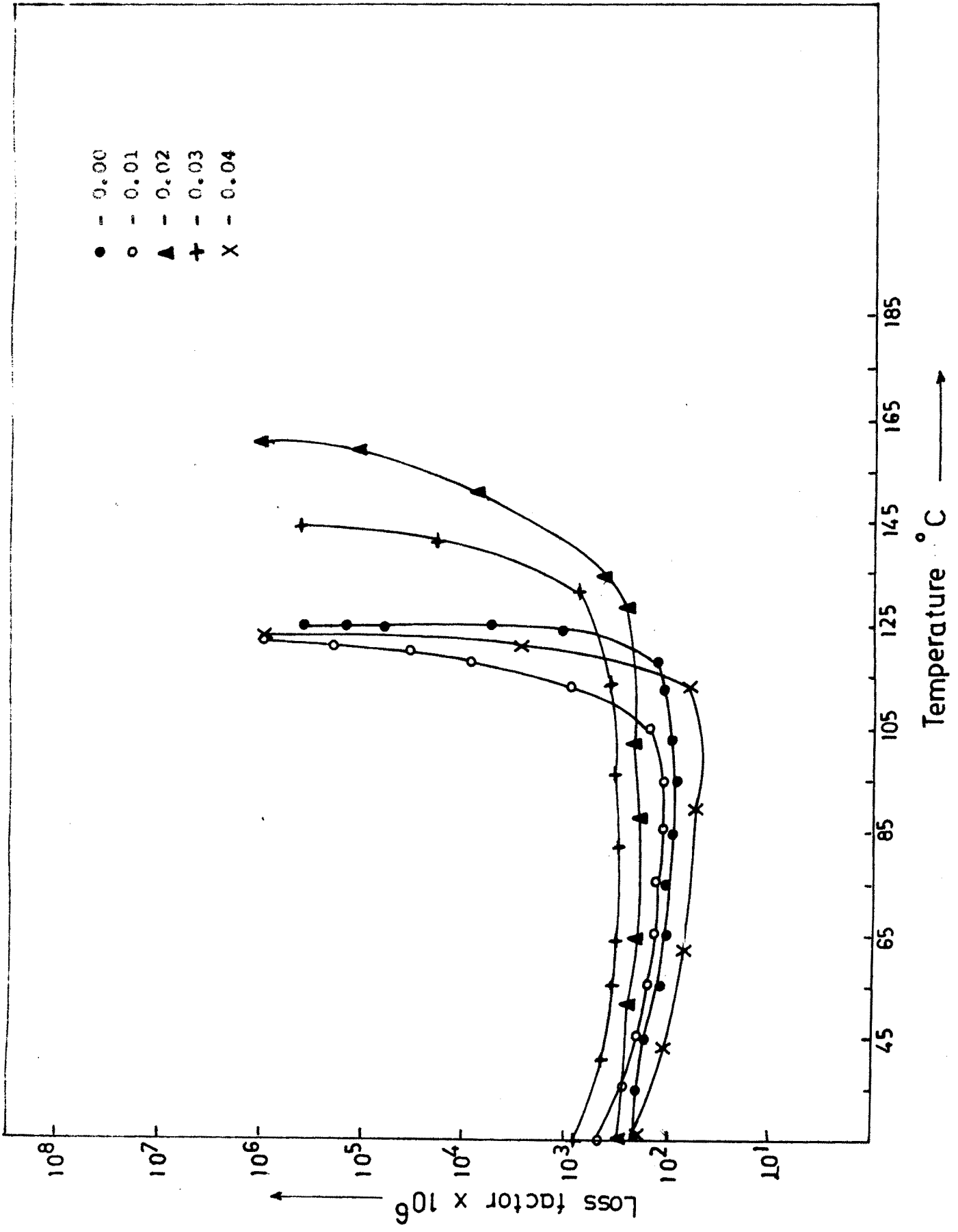


Fig. 3.14 : Thermal variation of Loss factor L.F. x 10<sup>6</sup> for Zn<sub>0.5</sub>Cu<sub>0.5-t</sub>Li<sub>2t</sub>Fe<sub>2</sub>O<sub>4</sub> .

losses are minimum in the frequency range of 10 KHz - 1 MHz as expected. Lithium ferrite is useful in microwave frequency region and the losses are minimum.

In figure 3.14 thermal variation of L.F. for the compositions  $Zn_{0.5}Cu_{0.5-t}Li_{2t}Fe_2O_4$  are shown. It is seen that L.F. decreases with increase in temperature range from 25°C to 115°C and for temperature greater than (115°C - 125°C) L.F. goes on increasing. On increasing the temperature  $\tan\delta$  tends to increase, the thermal variation of  $\tan\delta$  seems to be responsible for increase in L.F. In order to improve L.F. the ferrite can be operated at low temperatures.

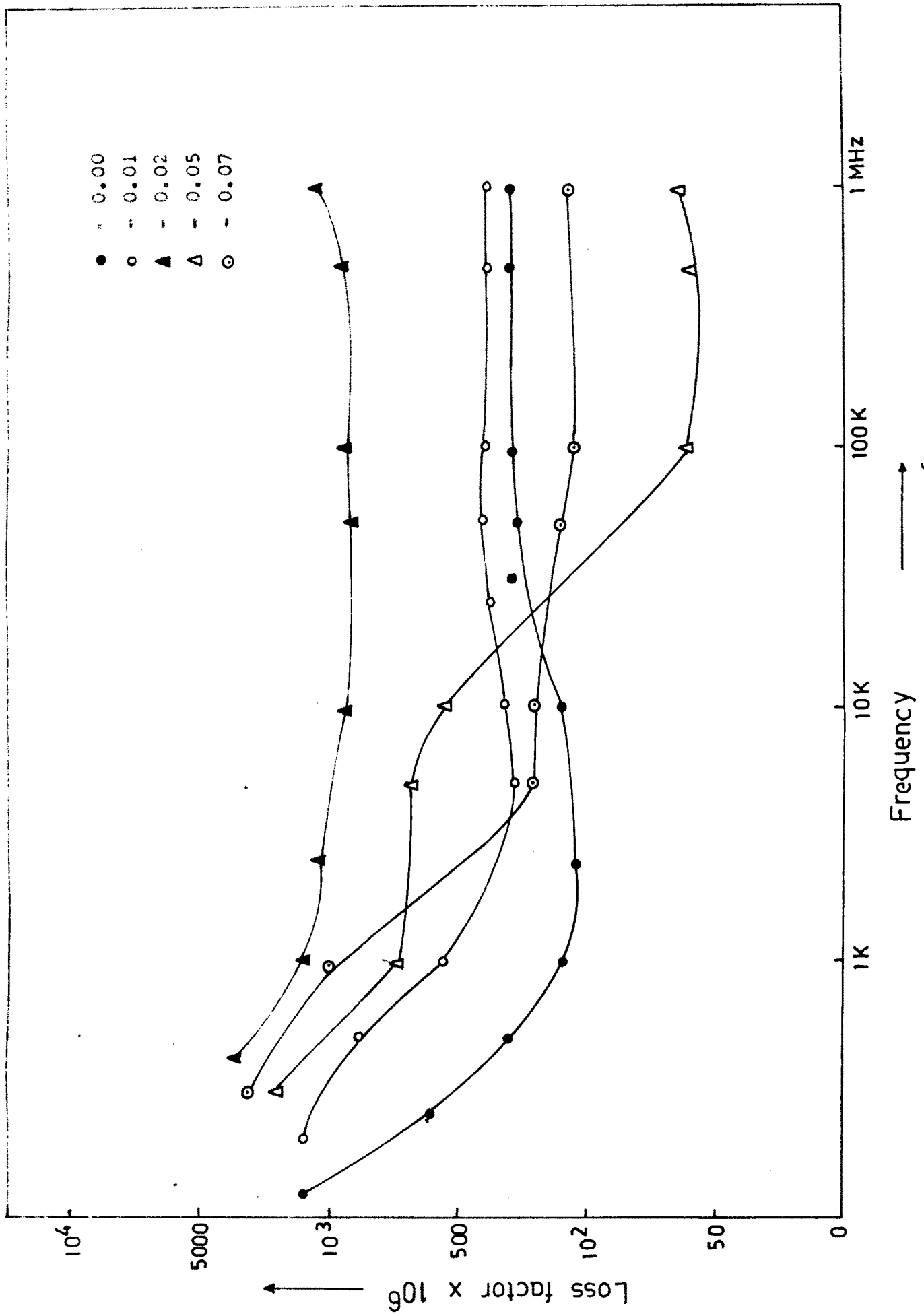


Fig. 3.13 : Frequency variation of Loss factor L.F.  $\times 10^6$  for  $Zn_{0.5}Cu_{0.5-t}Li_2tFe_2O_4$ .

References

1. Baldha G.D., Upadhyay R.V. and Kulkarni R.G., Mat. Res. Bull. 21, (1986), 1051 - 1055.
2. Patil B.L., Sawant S.R., and Patil S.A., Czech. J. Phys. 43, 1, (1993), 87 - 93.
3. Kulkarni R.G. and Upadhyay R.V., Mat. Lett., 4, 3, (1986) 168 - 170.
4. Murthy C.R.K., Likhite S.D., Deutsch E.K., and Murthy G.S., Phys. of Earth and Planetary Interior, 30, (1982), 281 - 290.
5. Steerstadt K., Benz H. and Rechenberg H., Proceedings of the International Conference on Magnetism, Nottingham, September (1964), 611.
6. Sawant S.R., Birajdar D.S., Suryavanshi S.S., Sankpal A.M., Patil B.L., Patil S.A. and Patil R.N., Indian J. Pure and Appl. Phys., Vol. 28, (1990), 424 - 426.
7. Neel L., Adv. Phys. 4, 191 (1955).
8. Radhakrishnamurthy C. and Nandikar N.G., Pramana Vol. 13, No. 4, pp. 413 - 422, Oct. (1979).
9. Hopkinson J. Phil. Trans. R. Soc. (London), A. 180, 443 (1989).
10. Chaugule R.S., Radhakrishnamurthy C., Sampathkumaran E.V., Malik S.K. and Vijayaraghavan R., Mat. Res. Bull. Vol. 18, 817 (1983).
11. Murthy C.R.K., Jr. Geologic Society of India, 26, (1985), 640 - 651.

12. Murthy C.R.K., Nandikar N.G., *Pramana*, 13 (4), (1979), 413 - 422.
13. Murthy V.R.K., Raman R. and Vishwanathan B., *Proceeding of ICF - 5, India*, (1989), 447 - 451.
14. Moye V., Rane K.S., Kamat Dalal V.N., Jr. *Mater. Sci., Mat. in Electronics*, 1, (1990), 212 - 218.
15. Kakatkar S.V., Kakatkar S.S., Patil R.S., Sankpal A.M., Suryavanshi S.S., Chaudhari N.D., and Sawant S.R., Jr. *of Magn. Mater.* 159 (1996), 361 - 366.
16. Jan Smit, "Magnetic properties of materials", Mac. Graw Hill Co., New York (1971).
17. Puri R.K., Mitra Reshmi and Mendiratta R.G., *Proceedings of ICF - 5 India* (1989), 353 - 357.
18. Argentina G.M., and Baba P.D., *IEEE Trans. Microwave Theory Technology* 22, (1972), 652.
19. Srivastava C.M., Shringi S.N., Srivastava R.G. and Nandikar N.G., *Phys. Rev. B.*, 14 (1976), 2032.
20. Zener C., *Phys. Rev.* 96 (1954) 13 - 35.
21. Dionne G.F., *J. Appl. Phys.*, 40 (1969) 431.
22. Goodenough J.B., *Phys. Rev.* 95, (1954) 917.
23. Goldman A., "Modern Ferrite Technology", Van Nostrand Reinhold; New York (1990) 89.
24. Jadhav S.R., Sawant S.R., Suryavanshi S.S. and Patil S.A., *J. Less Commn. Mat.*, 158, (1990) 199.

25. Murthy V.R.K., Raman R. and Vishwanath B., Proceedings of International Conference on Ferrites, ICF - 5, 1, (1989), 447.
26. Snelling E.C., "Soft Ferrites", Butterworths, (London) 1988, 309.
27. Bradley F.N., "Materials for Magnetic Functions", Hyden Book Co. Inc., D.B., Taraporewala Sons and Co. Pvt. Ltd., (1988).
28. Standley K.J., "Oxide Magnetic Materials", Clarendon Press, Oxford, (1972), 98.
29. Ghate B.B. and Goldman A., "Materials Science and Technology, A Comprehensive Treatment", edited by Cahn R.W., Haasen P., Kramer E.J., Vol. 11, Properties of Ceramics, Volume Editor M. Swain, VCH Verlag (1991) p.679.
30. Knowles J.E., J. Phys. (Paris), 38, (1977), (1 - 27).
31. Tanaka T., Japanese J. Appl. Phys. 17 (2), (1978), 349.
32. Stopples D.J., Appl. Phys. 51, (5), (1980) 2789.
33. Loaec J., J. Phys. D. Appl. Phys. 26, (1993), 963.
34. Globus A., and Duplex P., Physica Status Solidi, 31, (1969) 765.
35. Enz U., Proc. IEEE B, 109, (1962) 246.
36. Ohta K., J. Phys. Soc. Japan, 18, (1963) 685.
37. Rado G.T., Rev. Mod. Phys., 25 (1953), 81.
38. Rado G.T., Folen V.J. and Emerson W.H., Proc. Instn, Elect., Engrs, B 1045, (1957) 198.

39. Rado G.T. and Terries A., Phys. Rev. 88, (1952),  
909.
40. Rado G.T., Wright R.W., and Emerson W.H., Phys. Rev.  
80 (1950) 273.